

Energy Shaping Control of a CyberOctopus Soft Arm

Heng-Sheng Chang^{1,2}, Udit Halder², Chia-Hsien Shih¹, Arman Tekinalp¹, Tejaswin Parthasarathy¹, Ekaterina Gribkova³, Girish Chowdhary^{2,4}, Rhanor Gillette^{3,5}, Mattia Gazzola^{1,6,7}, Prashant G. Mehta^{1,2}

Abstract—This paper entails application of the energy shaping methodology to control a flexible, elastic Cosserat rod model. Recent interest in such continuum models stems from applications in soft robotics, and from the growing recognition of the role of mechanics and embodiment in biological control strategies: octopuses are often regarded as iconic examples of this interplay. Here, the dynamics of the Cosserat rod, modeling a single octopus arm, are treated as a Hamiltonian system and the internal muscle actuators are modeled as distributed forces and couples. The proposed energy shaping control design procedure involves two steps: (1) a potential energy is designed such that its minimizer is the desired equilibrium configuration; (2) an energy shaping control law is implemented to reach the desired equilibrium. By interpreting the controlled Hamiltonian as a Lyapunov function, asymptotic stability of the equilibrium configuration is deduced. The energy shaping control law is shown to require only the deformations of the equilibrium configuration. A forward-backward algorithm is proposed to compute these deformations in an online iterative manner. The overall control design methodology is implemented and demonstrated in a dynamic simulation environment. Results of several bio-inspired numerical experiments involving the control of octopus arms are reported.

Index Terms—Cosserat rod, Hamiltonian systems, energy-shaping control, soft robotics, octopus

I. INTRODUCTION

In recent years, the octopus has become an iconic example of the potential opportunities that lie in the use of soft, compliant materials in robotic applications, to enhance dexterity, safety, and body reconfiguration abilities [1], [2]. Indeed, the octopus and other soft-bodied animals are able to coordinate virtually infinite degrees of freedom into a rich repertoire of complex manipulation and motion patterns, from reaching, grasping, fetching, to crawling and swimming [3]–[5]. Recent proof-of-concept soft robots continue to highlight the need for theoretical and algorithmic control approaches that are specifically tailored to such distributed and compliant mechanical systems. This provides the motivation for the

We gratefully acknowledge financial support from ONR MURI N00014-19-1-2373 (G.C., M.G., M.G.P.), NSF/USDA #2019-67021-28989 (G.C., M.G.), and NSF EFRI C3 SoRo #1830881 (M.G.). We also acknowledge computing resources provided by the Blue Waters project (OCI-0725070, ACI-1238993), a joint effort of the University of Illinois at Urbana-Champaign and its National Center for Supercomputing Applications, and the Extreme Science and Engineering Discovery Environment (XSEDE) Stampede2 (ACI-1548562) at the Texas Advanced Computing Center (TACC) through allocation TG-MCB190004.

¹Department of Mechanical Science and Engineering, ²Coordinated Science Laboratory, ³Neuroscience Program, ⁴Department of Agricultural and Biological Engineering, ⁵Department of Molecular and Integrative Physiology, ⁶National Center for Supercomputing Applications, & ⁷Institute for Genomic Biology, University of Illinois at Urbana-Champaign. Corresponding e-mail: udit@illinois.edu

work reported in this paper where we apply energy shaping control techniques to control an octopus arm.

The dynamics of the arm are modeled using the Cosserat theory of elastic rods [6]. In contrast to typical rigid links model of classical robotics, Cosserat rod models capture, through linear and angular momentum balances, the (one-dimensional) continuum and distributed nature of elastic slender bodies deforming in space. These models account for all modes of deformation – bend, twist, stretch, shear – induced by external and internal forces and couples.

Our control-oriented viewpoint is to interpret the rod as a Hamiltonian system [7], [8] where the potential energy is expressed in terms of strains. This allows us to apply the energy shaping control design procedure that involves two steps: (1) a potential energy is designed such that its minimizer is the desired static equilibrium (encoding the octopus’ goal, e.g., reaching an object); (2) an energy shaping control law is implemented to achieve the desired equilibrium. In a standard manner, by interpreting the controlled Hamiltonian as a Lyapunov function, the equilibrium configuration is shown to be asymptotically stable.

The proposed procedure has several useful features. It yields a simple closed-form formula for the control law which is easily integrated in a realistic simulation. The modified potential energy and the controlled Hamiltonian have useful physical interpretations as modified stress-strain relationship. The simple control law provides a benchmark for more sophisticated forms of controls where additional constraints due to sensing and actuation may be taken into account. The algorithms described in this paper are demonstrated in a computational *CyberOctopus* which is being developed to simulate soft body mechanics coupled with distributed sensory-motor infrastructure operating in a realistic physical environment. The mechanics component of the CyberOctopus utilizes *Elastica*, an existing software for numerical modeling and simulation of three-dimensional Cosserat rods [9], [10]. Several reaching motion patterns inspired by results reported in the octopus’ literature are demonstrated in numerical experiments.

The outline of the remainder of this paper is as follows. The static and dynamic equations of the classical planar Cosserat theory are introduced in Sec. II. The section includes a self-contained discussion of an optimal control-type formulation of the rod statics and the Hamiltonian formulation of the rod dynamics. The proposed energy-shaping control design procedure appears in Sec. III. The details of the numerical simulation platform and the results of the numerical experiments appear in Sec. IV and Sec. V,

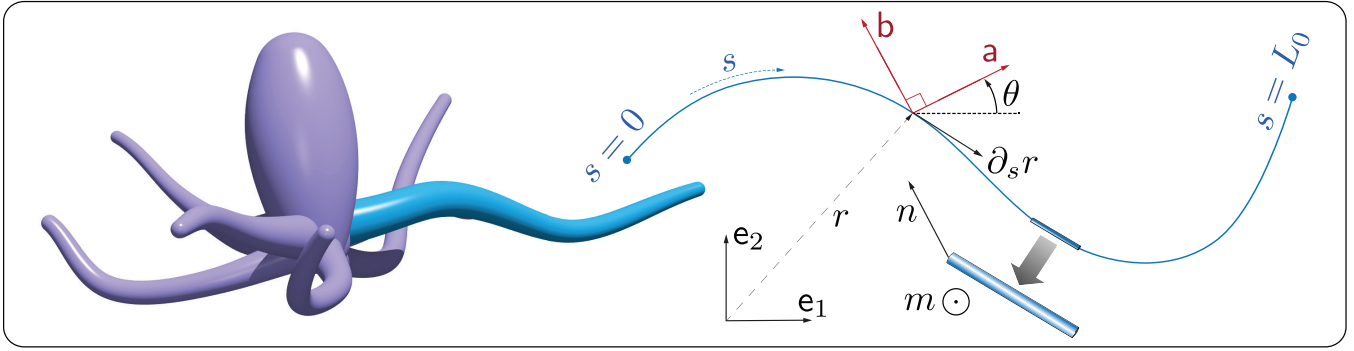


Fig. 1: Modeling an octopus arm as a special Cosserat rod

respectively. The conclusions and directions for future research are briefly described in Sec. VI.

II. COSSERAT ROD MODELS OF A SINGLE ARM

Let $\{e_1, e_2\}$ denote a fixed orthonormal basis for the two-dimensional lab frame¹. In its reference undeformed configuration, the rod is of length L_0 and lies parallel to the e_1 axis. The independent coordinates are time $t \in \mathbb{R}$ and the arc-length of the centerline $s \in [0, L_0]$. The partial derivatives with respect to t and s are denoted as ∂_t and ∂_s , respectively. The *state* of the rod is described by the vector-valued function q (Fig. 1)

$$q(s, t) := \begin{bmatrix} x(s, t) \\ y(s, t) \\ \theta(s, t) \end{bmatrix}$$

where $r = (x, y) \in \mathbb{R}^2$ denotes the position vector of the centerline, and the angle $\theta \in \mathbb{R}$ defines a material frame spanned by the orthonormal pairs $\{a, b\}$, where $a = \cos \theta e_1 + \sin \theta e_2$, $b = -\sin \theta e_1 + \cos \theta e_2$. The vector a is normal to the cross section: it captures the shear deformations whereby the cross section ‘shears’ relative to the tangent of the centerline.

A. Statics – an optimal control viewpoint

The statics of the rod require consideration of the rod’s potential energy denoted as \mathcal{V} . It is a functional of the strains, i.e., curvature, stretch and shear. Strains are related to the local frame $\{a, b\}$ through $\partial_s r = \nu_1 a + \nu_2 b$, where ν_1 and ν_2 represent stretch and shear, respectively. The curvature $\kappa := \partial_s \theta$ completes the triad of deformations $w := (\nu_1, \nu_2, \kappa)$ that fully characterizes the rod’s kinematics

$$\partial_s q = f(q, w) := \begin{bmatrix} \nu_1 \cos \theta - \nu_2 \sin \theta \\ \nu_1 \sin \theta + \nu_2 \cos \theta \\ \kappa \end{bmatrix} \quad (1)$$

and potential energy

$$\mathcal{V}(q) = \int_0^{L_0} W(w(s)) ds$$

¹Although all the considerations of this paper are applicable to the general three-dimensional (3D) Cosserat rod models, we provide the exposition for two-dimensional (2D) models. The notation is simpler and the key ideas are communicated more easily to a broader audience.

where $W : (\nu_1, \nu_2, \kappa) \mapsto \mathbb{R}$ is the energy stored in the rod because of its mechanical deformation. Under the assumption of a perfectly elastic material characterized by a linear stress-strain relation, W takes the quadratic form

$$W = \frac{1}{2} (EA(\nu_1 - \nu_1^\circ)^2 + GA(\nu_2 - \nu_2^\circ)^2 + EI(\kappa - \kappa^\circ)^2) \quad (2)$$

where E and G are the material Young’s and shear moduli, A and I are the cross sectional area and second moment of area, and $\nu_1^\circ, \nu_2^\circ, \kappa^\circ$ are the intrinsic deformations that determine the rod’s shape at rest. If $\nu_1^\circ \equiv 1, \nu_2^\circ \equiv 0, \kappa^\circ \equiv 0$, then the rest configuration is a straight undeformed rod.

The statics of the rod admit an interesting optimal control re-formulation; c.f., [11], [12]. Any static configuration of the rod is a stationary point of the potential energy \mathcal{V} with the constraint expressed by (1)

$$\underset{w(\cdot)}{\text{minimize}} \quad \mathcal{V} = \int_0^{L_0} W(w(s)) ds, \quad (3)$$

$$\text{subject to } \partial_s q = f(q, w), \quad \text{with } q(0) = q_0, \quad q(L_0) = q_1$$

Here, q_0 and q_1 are the states of the rod at the base ($s = 0$) and at the tip ($s = L_0$). Desired static configurations of the rod are obtained via the application of the Pontryagin’s Maximum Principle (PMP). Write the control Hamiltonian as

$$H(q, \lambda, w) = \lambda^\top f(q, w) - W(w) \quad (4)$$

where $\lambda(s) = (\lambda_1(s), \lambda_2(s), \lambda_3(s))^\top \in \mathbb{R}^3$ is the costate vector. The Hamilton’s equations are given by

$$\partial_s q = \frac{\partial H}{\partial \lambda} = f(q, w) \quad (5)$$

$$\begin{aligned} \partial_s \lambda &= -\frac{\partial H}{\partial q} \\ &= \begin{bmatrix} 0 \\ 0 \\ \{-\nu_1(-\lambda_1 \sin \theta + \lambda_2 \cos \theta) \\ + \nu_2(\lambda_1 \cos \theta + \lambda_2 \sin \theta)\} \end{bmatrix} =: g(q, \lambda, w) \end{aligned} \quad (6)$$

The optimal deformations are obtained by pointwise maximization of the Hamiltonian (4). For the quadratic choice of

the stored energy function W , the maximization yields

$$\begin{bmatrix} EA(\nu_1 - 1) \\ GA\nu_2 \\ EI\kappa \end{bmatrix} = \begin{bmatrix} \lambda_1 \cos \theta + \lambda_2 \sin \theta \\ -\lambda_1 \sin \theta + \lambda_2 \cos \theta \\ \lambda_3 \end{bmatrix} \quad (7)$$

Remark 1: In Cosserat rod theory, Eq. (5)-(6) are the well known static equations. The costate variables (λ_1, λ_2) and λ_3 represent, respectively, the internal forces and couple in the laboratory frame. In the material frame, the internal forces and couple are denoted as $(n_1, n_2, m) := (\lambda_1 \cos \theta + \lambda_2 \sin \theta, -\lambda_1 \sin \theta + \lambda_2 \cos \theta, \lambda_3)$. Equation (7) provides a relationship between the deformations and these internal forces and couple. More generally,

$$n_i = \frac{\partial W}{\partial \nu_i}, i = 1, 2, \quad m = \frac{\partial W}{\partial \kappa}$$

are referred to as the *constitutive laws* or the load-strain relationships that characterize the material of the rod.

Remark 2: The optimal control formulation (3) is easily extended to handle constraints in the environment, such as boundaries defined by ground or physical obstacles. The mathematical modeling and incorporation of these constraints is the subject of Sec. III-C.

B. Dynamics – the Hamiltonian form

In a dynamic setting, the state $q = (x, y, \theta)$ is a function of both s and t . Let $p = M\partial_t q$ denote the momentum, where $M = \text{diag}(\rho A, \rho A, \rho I)$ is the inertia matrix and ρ is the material density. The kinetic energy is expressed as

$$\mathcal{T} = \frac{1}{2} \int_0^{L_0} (\rho A((\partial_t x)^2 + (\partial_t y)^2) + \rho I(\partial_t \theta)^2) ds$$

The Hamiltonian is the total energy of the system, $\mathcal{H}(q, p) = \mathcal{T}(p) + \mathcal{V}(q)$.

In the absence of external forces and couples, the dynamics of the rod are described by Hamilton's equations of classical mechanics

$$\begin{aligned} \frac{dq}{dt} &= \frac{\delta \mathcal{H}}{\delta p} = M^{-1}p \\ \frac{dp}{dt} &= -\frac{\delta \mathcal{H}}{\delta q} = -\frac{\delta \mathcal{V}}{\delta q} \end{aligned} \quad (8)$$

The evolution equation (8) requires the specification of boundary conditions at $s = 0$ and $s = L_0$ as well as initial conditions at $t = 0$. These together with the explicit form of the dynamic equations of the rod, appear in Sec. IV.

III. CONTROL DESIGN

Muscles in the arm generate distributed internal forces and torques that determine the dynamics and shape of the arm itself. Such internal loads are employed here as the control vector u . The Hamiltonian control system is expressed as

$$\begin{aligned} \frac{dq}{dt} &= \frac{\delta \mathcal{H}}{\delta p} \\ \frac{dp}{dt} &= -\frac{\delta \mathcal{H}}{\delta q} + u \end{aligned}$$

The control problem is to design a feedback control law for u to displace and stabilize the tip of the rod ($s = L_0$) to a specified target location $q^* \in \mathbb{R}^3$.

A. Energy shaping control law

The idea is to shape the potential energy of the rod, using techniques from the port-Hamiltonian control theory [13]–[15]. For this purpose, suppose one can design a potential energy, denoted as \mathcal{V}^d , whose minimizer (static equilibrium) achieves the desired control objective². Then the following proposition gives an explicit form of the control law:

Proposition 3.1: Let $\mathcal{V}^d(q)$ denote a desired potential energy function with minimum at a configuration \bar{q} . Then the control law

$$u = -\frac{\delta}{\delta q}(\mathcal{V}^d - \mathcal{V}) - \gamma M^{-1}p, \quad \gamma > 0 \quad (9)$$

renders the point $(\bar{q}, 0)$ asymptotically stable.

A sketch of the proof (adapted from [13]) is provided next. The control law (9) serves to modify the potential energy of the system to \mathcal{V}^d

$$\frac{dq}{dt} = \frac{\delta \bar{\mathcal{H}}}{\delta p}, \quad \frac{dp}{dt} = -\frac{\delta \bar{\mathcal{H}}}{\delta q} - \gamma M^{-1}p \quad (10)$$

where

$$\bar{\mathcal{H}}(q, p) = \mathcal{T}(p) + \mathcal{V}^d(q)$$

is the modified control Hamiltonian. Now, $\bar{\mathcal{H}}(q, p) \geq 0$ for all (q, p) , $\bar{\mathcal{H}} = 0$ only at $(\bar{q}, 0)$ and along a solution trajectory of (10) we have

$$\frac{d\bar{\mathcal{H}}}{dt} = -\gamma \left\langle \frac{dq}{dt}, \frac{dq}{dt} \right\rangle \leq 0$$

where the inner product above is taken in the L^2 sense. This shows that the total energy of the system is non-increasing. By an application of the LaSalle's theorem, the solution converges to the largest invariant subset of $\left\{ (q, p) \mid \frac{d\bar{\mathcal{H}}}{dt} = 0 \right\}$ which is $(\bar{q}, 0)$. A rigorous application of LaSalle principle also requires one to show that the trajectories of the nonlinear semigroup of (10) are precompact or relatively compact in an appropriate function space. This remains to be verified.

Remark 3: A justification of the small dissipation term in (10) can be provided in variety of ways, for example it can be physically assimilated to material viscoelastic effects.

It remains to determine the desired potential energy. This is the subject of the next section.

B. Design of desired potential energy

In order to move the arm tip to a desired location q^* , a natural choice is to consider the problem (3) with $q(L_0) = q^*$. A more practical approach – for the purposes of algorithm design and implementation – is to consider the following modified version of the problem (3)

$$\text{minimize}_{w(\cdot)} J = \int_0^{L_0} W(w(s)) ds + \mu \Phi(q(L_0), q^*) \quad (11)$$

subject to $\partial_s q = f(q, w)$, with $q(0) = q_0$

²The design of the desired potential energy is the subject of the following sub-section.

where the terminal cost Φ is used to penalize the deviation of the tip from the desired location, and μ is a positive parameter. The optimality conditions (6)-(7) now also include the transversality condition

$$\lambda(L_0) = -\mu \frac{\partial \Phi}{\partial q}(q(L_0), q^*) \quad (12)$$

Suppose problem (11) can be solved to obtain the static solution \bar{q} . Then one possible approach to determine the desired potential energy function \mathcal{V}^d is as follows. The function \mathcal{V}^d must be positive definite $\mathcal{V}^d(q) > 0$ for all $q \neq \bar{q}$, and $\mathcal{V}^d(\bar{q}) = 0$. We consider the simple formula for \mathcal{V}^d

$$\mathcal{V}^d(q) = \frac{1}{2} \int_0^{L_0} (EA(\nu_1 - \bar{\nu}_1)^2 + GA(\nu_2 - \bar{\nu}_2)^2 + EI(\kappa - \bar{\kappa})^2) ds \quad (13)$$

where $(\bar{\nu}_1, \bar{\nu}_2, \bar{\kappa})$ represent the optimal deformations corresponding to the solution \bar{q} of the control problem (11).

Using this choice yields the following explicit form of the energy shaping control law

$$u = - \left[\frac{\partial}{\partial s} \left(\begin{pmatrix} \cos \theta & -\sin \theta \\ \sin \theta & \cos \theta \end{pmatrix} \begin{pmatrix} EA(\bar{\nu}_1 - 1) \\ GA\bar{\nu}_2 \end{pmatrix} \right) \right] - \gamma \partial_t q \quad (14)$$

Physically, this procedure is equivalent to artificially replacing the intrinsic strains of (2) with the optimal deformations $(\bar{\nu}_1, \bar{\nu}_2, \bar{\kappa})$. The energy shaping form of the controlled Hamiltonian dynamics then takes care of generating the control inputs (which may be interpreted as internal stresses) required to bring the rod to its new equilibrium configuration.

C. Additional constraints in the environment

Physical boundaries such as ground surfaces or obstacles are mathematically modeled as inequalities that provide additional constraints to the optimal control problem (11)

$$\Psi_j(q) \leq 0, \quad j = 1, 2, \dots, N_{\text{obs}}$$

Following [16], the constrained optimal control problem is solved by augmenting the states q with N_{obs} additional states, denoted as \hat{q}_j for $j = 1, \dots, N_{\text{obs}}$. The model of each additional state is defined as

$$\partial_s \hat{q}_j = c_j(q) = \max(\Psi_j(q), 0), \quad \hat{q}_j(0) = 0$$

Note that $c_j(q)$ is non-negative for each j . The terminal value $\hat{q}_j(L_0)$ is referred to as the performance index. It indicates the degree to which the j -th inequality constraint has been violated along the length of the rod. To minimize the performance index, the terminal cost function is modified as follows

$$\hat{\Phi}(q(L_0), \hat{q}(L_0)) = \Phi(q(L_0)) + \sum_{j=1}^{N_{\text{obs}}} \xi_j \hat{q}_j(L_0)$$

where $\xi_j > 0$ is the weight for the performance index $\hat{q}_j(L_0)$.

The Hamilton's equations of the state and the pointwise maximization condition for the Hamiltonian are exactly the

same as before. The equation for costates are modified to now also include an additional term on account of the constraints

$$\partial_s \lambda = -\frac{\partial H}{\partial q} + \sum_{j=1}^{N_{\text{obs}}} \xi_j \frac{\partial c_j(q)}{\partial q}$$

D. Algorithm

In summary, the proposed design procedure involves two steps. In step 1, the optimal deformations are determined by solving the Hamilton's equation for the static problem with possible additional constraints due to obstacles. In step 2, the energy shaping control law (14) is implemented to achieve the desired objective.

There are a number of ways to numerically solve the Hamilton's equations. Offline approaches include the use of a shooting method to solve the two point boundary value problem (BVP) [17], or using μ as a continuation parameter based on the methods proposed in [18]. Once the optimal deformations are obtained, the control law is implemented directly using (14).

Envisioning the control of a *CyberOctopus* which interacts with a dynamic environment, an online approach is more appropriate. In this case, step 1 is implemented to solve the BVP iteratively, interspersing every iteration with step 2 directly within the simulation of the dynamic model. For the iterative solution of the BVP problem, a gradient ascent algorithm is used to update (or learn) the optimal deformations as follows

$$\frac{dw}{dt} = \eta(t) \frac{\partial H}{\partial w}(q, \lambda, w) \quad (15)$$

where $\eta(t)$ is the update stepsize (or learning rate). For each t , the states are integrated forward from the initial condition q_0 , while the costates are integrated backward from the terminal condition (12). This algorithm is known in literature as forward-backward algorithm for optimal control [19], [20], and is presented in Algorithm 1. Convergence results typically require sufficiently small values of the step size parameter η .

IV. COSSERAT ROD MODEL DISCRETIZATION

The explicit form of the equations of motion of a planar Cosserat rod [6] are as follows:

$$\begin{aligned} \partial_t(\rho A \partial_t r) &= \partial_s n + F \\ \partial_t(\rho I \partial_t \theta) &= \partial_s m + \nu_1 n_2 - \nu_2 n_1 + C \end{aligned} \quad (16)$$

where $n = n_1 \mathbf{a} + n_2 \mathbf{b}$ and m are internal forces and couple, respectively, and $u = (F, C)$ are external forces and couple per unit length, which are employed here as control variables. We fix the rod base ($s = 0$) at the origin while the tip ($s = L_0$) is free to move. Then, the initial (17) and boundary (18) conditions that accompany the dynamics (16) are

$$r(s, 0) = r^\circ(s), \quad \theta(s, 0) = 0, \quad \partial_t r(s, 0) = 0, \quad \partial_t \theta(s, 0) = 0 \quad (17)$$

$$r(0, t) = 0, \quad \theta(0, t) = 0, \quad n(L_0, t) = 0, \quad m(L_0, t) = 0 \quad (18)$$

where $r^\circ(s) = (s, 0)$ is the initial position vector.

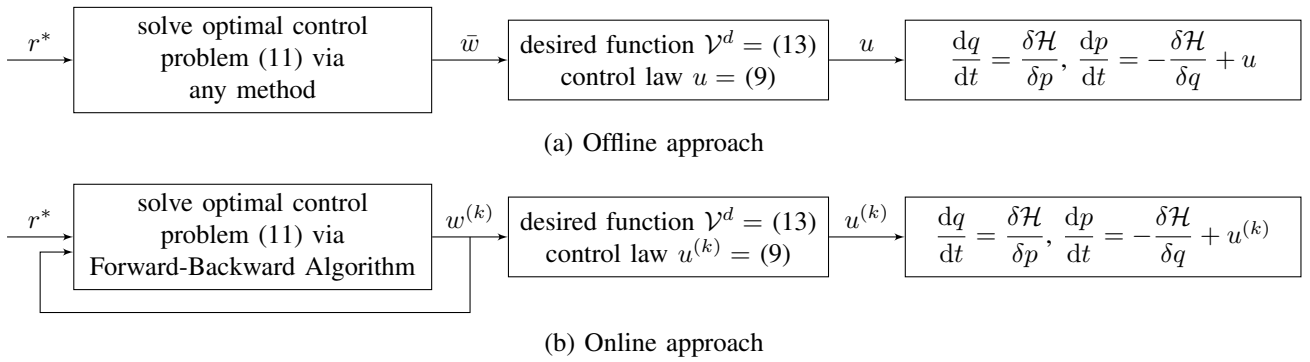


Fig. 2: (a) Offline approach. The block on the very left is the first step which takes the target position r^* as input and outputs target deformation \bar{w} . The middle block is the second step which constructs u by following the control law (9). Lastly, the system will be stabilized at the target deformation once the control is applied. (b) Online approach. The two-step procedure here is similar to (a) except for the fact that the deformations are updated iteratively, and $w^{(k)}$ is used to compute the energy shaping control $u^{(k)}$.

Algorithm 1 Forward-Backward Algorithm

Input: Terminal cost function $\mu\Phi(q(L_0), q^*)$

Output: Optimal deformations $\bar{w} = (\bar{v}_1, \bar{v}_2, \bar{\kappa})$

- 1: Initialize: deformations $w^{(0)}$, states at base ($s = 0$) q_0
- 2: **for** $k = 0$ to MaxIter **do**
- 3: Update forward (1):

$$q^{(k)}(s) = q_0 + \int_0^s f(q^{(k)}(s), w^{(k)}(s)) ds$$

- 4: Update backward (12), (6):

$$\lambda^{(k)}(L_0) = -\mu \frac{\partial \Phi}{\partial q}(q^{(k)}(L_0), q^*)$$

$$\lambda^{(k)}(s) = \lambda^{(k)}(L_0) - \int_s^{L_0} g(q^{(k)}(s), w^{(k)}(s)) ds$$

- 5: Update deformations (15):

$$w^{(k+1)} = w^{(k)} + \eta_k \frac{\partial H}{\partial w}(q^{(k)}, \lambda^{(k)}, w^{(k)}) \Delta t$$

- 6: **end for**

- 7: Output the final deformations as \bar{w}
-

In all our demonstrations, the arm is initially straight, undeformed and at rest. In order to mimic the tapered geometry of an actual octopus arm, we employed a rod with the variable diameter profile $\phi(s) = \phi_{\text{tip}}s + \phi_{\text{base}}(L_0 - s)$. The cross section area and the second moment of the area are calculated as $A = \frac{\pi\phi^2}{4}$, $I = \frac{A^2}{4\pi}$. The arm dimensions of a live octopus (*O. rubescens*), such as length and the diameters along the arm, were measured in a laboratory environment with the help of camera recordings. Elastic moduli of biological tissue [21] are used for our simulations. The simulation parameters are listed in Table I.

The Cosserat governing equations are solved numerically using our open-source, dynamic, three-dimensional (3D) simulation framework *Elastica* [9], [10]. In the context of this work, we constrained all variables and motions within

TABLE I: Parameters

Parameter	Description	Value
Numerical Simulation		
L_0	total length of an undeformed arm [cm]	20
ϕ_{base}	base diameter [cm]	2
ϕ_{tip}	tip diameter [cm]	0.04
E	Young's modulus [kPa]	10
G	shear modulus [kPa]	1
ρ	density [kg/m ³]	700
γ	dissipation [kg/s]	0.01
N	discrete number of elements	100
Δt	discrete time-step [s]	10^{-5}
Forward-Backward Algorithm		
μ	regularization parameter	10^3
η	learning rate	0.01
ξ	weight for the performance index	10^5

a prescribed plane, which acts as a fixed-point space for the dynamics. In *Elastica*, the rod is decomposed into $(N + 1)$ vertices hosting translational degrees of freedom (r), and N connecting cylindrical segments hosting rotational degrees of freedom (θ). All spatial operators are discretized using second-order finite-differences. The resulting discretized system of equations is evolved in time using a second-order Verlet scheme. Additional forces and torques, such as those arising from contact with objects in the environment, are included in this model as forcing terms, similar to the control u . The method has been validated against a number of benchmark problems with known analytical solutions [9]. Moreover, it has been shown to successfully capture the dynamics of a wide range of biophysical phenomena from complex musculoskeletal architectures [10] and bio-hybrid robots [22], [23] to artificial muscles [24] and meta-materials [25]. Further numerical details can be found in the above references.

V. NUMERICAL EXPERIMENTS

In the following we demonstrate the capabilities of our control approach via a set of numerical experiments inspired

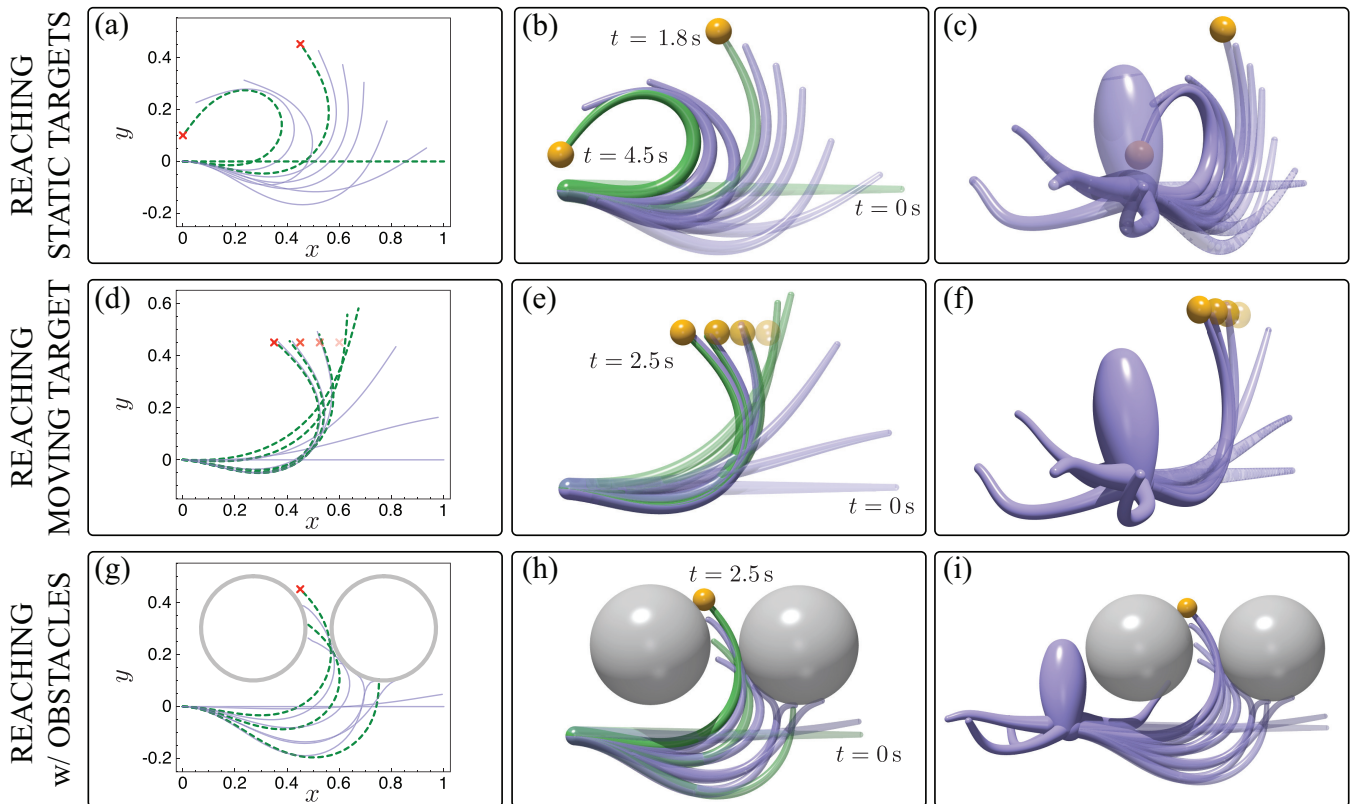


Fig. 3: Arm reaching control tasks. (a-c) The arm is tasked to reach two different locations one after the other, mimicking an octopus fetching a food source and bringing it back to its mouth. (a) Targets are located at $r^* = (9, 9)$ and $(0, 2)$ [cm] (axes normalized by undeformed arm length L_0) and indicated as red crosses. In (b – arm front view) and (c – octopus 3D rendering) targets are represented as orange spheres. Optimal arm configurations are depicted in green, while actual arm shapes evolution in time are depicted in purple. (d-e) The arm is tasked to reach a moving target, initially located at $(12, 9)$ [cm]. (g-i) The arm is tasked to reach a static target accounting for the presence of two identical solid spheres (grey) of 8 [cm] diameter, and located at $(5.4, 6)$ and $(15.4, 6)$ [cm]. The position of the static target is $r^* = (9, 9)$ [cm].

by arm reaching motions reported in octopus’ literature.

A. Reaching multiple static targets

Octopuses have been observed [3], [4], [26] to demonstrate stereotypical reaching and fetching motion, i.e. reaching to a food source by bend propagation and bringing it back to its mouth by forming a pseudo-joint in its arm. Inspired by this, our first experiment is conceptualized for the *CyberOctopus* elastic arm to mimic this kind of behavior. Given one or multiple static targets r^* , indicated as orange spheres, the goal of this numerical experiment is to reach each target with the tip of the arm one after the other. The first step is using the forward-backward algorithm to calculate offline (Fig. 2a) the static configuration, given each target’s position. To find the static configuration that allows the tip of the arm to reach the target, we set the terminal cost in the optimal control problem (11) as

$$\Phi(q(L_0), r^*) = \frac{1}{2} |r^* - r(L_0)|^2$$

There is no cost associated with $\theta(L_0)$ since the angle at which the tip captures the target is not of concern. The

transversality condition (12) becomes

$$\lambda(L_0) = \begin{bmatrix} \mu(x^* - x(L_0)) \\ \mu(y^* - y(L_0)) \\ 0 \end{bmatrix}$$

After computing the target configuration, we apply the explicit muscle forces and couples of (14), which smoothly bring the arm into its target shape. When the tip reaches the first target, another set of muscle forces and couples based on next target is applied. Therefore, the arm reaches each target one by one, as shown in Fig. 3a-c.

B. Reaching a moving target

Next, we consider reaching a moving target so that r^* is now an explicit function of time, mimicking the capture of a swimming prey [27], [28]. This scenario sets the stage for future investigations of capture strategies in more complex settings, for example accounting for preys’ evasion maneuvers. Thus, a method that continuously updates the desired arm configuration $\bar{q}(t)$ in response to dynamic targets becomes necessary, and we resort to the online control method of Fig. 2b.

In this test case, the target position is displaced as $r^*(t) = r^*(k\Delta t)$, where k is the iteration number. The target is

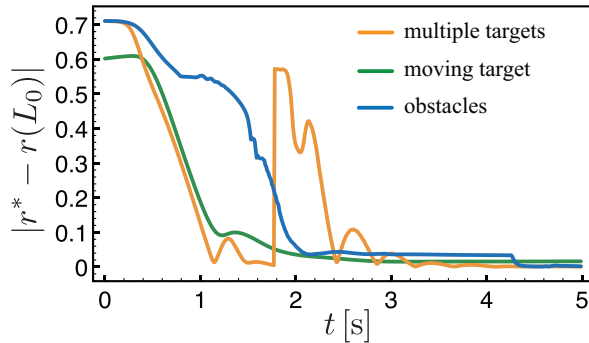


Fig. 4: Time-series plot of the distance (normalized by L_0) between the arm tip and the target position. The orange line corresponds to experiment A. The arm tip reaches the first target at 1.8 [s] and stabilizes at the second one after 4.5 [s]. The green line corresponds to experiment B, which becomes close to zero after 2.5 [s] as the tip of the arm chases and catches the moving target. The blue line corresponds to experiment C. During the period from 1 [s] to 2 [s], the tip slides against the obstacles, after which it is able to reach the target.

assumed to be moving at a constant velocity of 1 [cm/s], towards the $-e_1$ direction. It is to be noted that the controller for the arm does not know the velocity explicitly, instead it is assumed to know the position of the target at each time. This can be justified since the octopus can use visual cues and chemical signals to estimate the location of the prey. As can be seen in Fig. 3d-f, the tip of the arm catches the moving target, gradually morphing through a sequence of desired shapes.

C. Reaching with obstacles

Challenged with physical constraints, octopuses are known to adapt to the environment to accomplish complex tasks like reaching to a target [29], or solving puzzles [30]. For our final experiment, we consider the presence of solid obstacles to mimic an octopus operating in an anisotropic environment. The target is assumed to be static. We follow the method described in Sec. III-C to find optimal static configurations that respects the inequality constraints associated with hard boundaries, here represented by two spheres located in the arm plane. Thus, the inequality constraints are

$$\Psi_j(q(s, t)) = \left(\frac{\phi_j + \phi(s)}{2} \right)^2 - |r_j - r(s, t)|^2, \quad j = 1, 2$$

where ϕ_j is the diameter of the j -th sphere and r_j is its center position. The online control method (Fig. 2b) is then applied to calculate the energy-shaping control. The results of algorithm and simulations are shown in Fig. 3g-i, which illustrate how the tip avoids boundaries as the arm complies with the obstacles, sliding through them to finally reach the target.

Remark 4: In order to better understand the temporal performance of our control method, we plot the distance between the tip of the rod and the target position in Fig. 4. Some Reinforcement Learning (RL) and adaptive control

based algorithms are known to result in oscillations around the target. Compared with the manipulator results of RL based methods [31], our proposed energy shaping control method offers the system a stable equilibrium without the tip jittering near the target.

VI. CONCLUSION AND FUTURE WORK

In this paper, we have used the Cosserat rod theory to model a flexible octopus arm in a plane. Hamiltonian formulation of the dynamics of the rod is exploited to synthesize an energy-shaping control law that stabilizes the rod to a predefined deformed state. We have shown that an optimal control formulation yields a systematic way to compute desired static configuration. This also enables us to tackle obstacles. An iterative forward-backward algorithm is proposed so that it can be used online to calculate the energy-shaping control in the dynamic simulation of the rod. Numerical results demonstrate efficacy of this control scheme. As a direct extension, this idea can be applied to the general 3D case. In this work, a simplistic model of actuation is assumed. Future work will consider more realistic muscle actuation models, to solve manipulation problems in a biophysically realistic fashion.

REFERENCES

- [1] C. Laschi, M. Cianchetti, *et al.*, "Soft robot arm inspired by the octopus," *Advanced Robotics*, vol. 26, no. 7, pp. 709–727, 2012.
- [2] S. Min, J. Won, *et al.*, "Softcon: Simulation and control of soft-bodied animals with biomimetic actuators," *ACM Transactions on Graphics*, vol. 38, no. 6, 2019.
- [3] G. Sumbre, Y. Gutfreund, *et al.*, "Control of octopus arm extension by a peripheral motor program," *Science*, vol. 293, no. 5536, pp. 1845–1848, 2001.
- [4] G. Sumbre, G. Fiorito, *et al.*, "Motor control of flexible octopus arms," *Nature*, vol. 433, no. 7026, p. 595, 2005.
- [5] G. Levy, N. Neshet, *et al.*, "Motor control in soft-bodied animals: the octopus," in *The Oxford Handbook of Invertebrate Neurobiology*, 2017.
- [6] S. S. Antman, *Nonlinear Problems of Elasticity*. Springer, 1995.
- [7] J. C. Simo, J. E. Marsden, and P. S. Krishnaprasad, "The Hamiltonian structure of nonlinear elasticity: the material and convective representations of solids, rods, and plates," *Archive for Rational Mechanics and Analysis*, vol. 104, no. 2, pp. 125–183, 1988.
- [8] D. Dichmann, J. Maddocks, and R. Pego, "Hamiltonian dynamics of an elastica and the stability of solitary waves," *Archive for Rational Mechanics and Analysis*, vol. 135, no. 4, pp. 357–396, 1996.
- [9] M. Gazzola, L. Dudte, *et al.*, "Forward and inverse problems in the mechanics of soft filaments," *Royal Society Open Science*, vol. 5, no. 6, p. 171628, 2018.
- [10] X. Zhang, F. K. Chan, *et al.*, "Modeling and simulation of complex dynamic musculoskeletal architectures," *Nature Communications*, vol. 10, no. 1, pp. 1–12, 2019.
- [11] T. Bretl and Z. McCarthy, "Quasi-static manipulation of a Kirchhoff elastic rod based on a geometric analysis of equilibrium configurations," *The International Journal of Robotics Research*, vol. 33, no. 1, pp. 48–68, 2014.
- [12] J. Till and D. C. Rucker, "Elastic stability of cosserat rods and parallel continuum robots," *IEEE Transactions on Robotics*, vol. 33, no. 3, pp. 718–733, 2017.
- [13] M. Takegaki and S. Arimoto, "A new feedback method for dynamic control of manipulators," *Journal of Dynamic Systems, Measurement, and Control*, vol. 103, no. 2, pp. 119–125, 1981.
- [14] R. Ortega, A. J. Van Der Schaft, *et al.*, "Putting energy back in control," *IEEE Control Systems Magazine*, vol. 21, no. 2, pp. 18–33, 2001.
- [15] A. van der Schaft, *L2-gain and passivity techniques in nonlinear control*. Springer, 2000.

- [16] W. Mekarapiruk and R. Luus, "Optimal control of inequality state constrained systems," *Industrial & Engineering Chemistry Research*, vol. 36, no. 5, pp. 1686–1694, 1997.
- [17] D. D. Morrison, J. D. Riley, and J. F. Zancanaro, "Multiple shooting method for two-point boundary value problems," *Communications of the ACM*, vol. 5, no. 12, pp. 613–614, 1962.
- [18] T. J. Healey and P. G. Mehta, "Straightforward computation of spatial equilibria of geometrically exact cosserat rods," *International Journal of Bifurcation and Chaos*, vol. 15, no. 3, pp. 949–965, 2005.
- [19] M. McAsey, L. Mou, and W. Han, "Convergence of the forward-backward sweep method in optimal control," *Computational Optimization and Applications*, vol. 53, no. 1, pp. 207–226, 2012.
- [20] A. Taghvaei, J. W. Kim, and P. Mehta, "How regularization affects the critical points in linear networks," in *Advances in Neural Information Processing Systems*, 2017, pp. 2502–2512.
- [21] F. Tramacere, A. Kovalev, *et al.*, "Structure and mechanical properties of octopus vulgaris suckers," *Journal of The Royal Society Interface*, vol. 11, no. 91, p. 20130816, 2014.
- [22] G. Pagan-Diaz, X. Zhang, *et al.*, "Simulation and fabrication of stronger, larger, and faster walking biohybrid machines," *Advanced Functional Materials*, vol. 28, no. 23, p. 1801145, 2018.
- [23] O. Aydin, X. Zhang, *et al.*, "Neuromuscular actuation of biohybrid motile bots," *Proceedings of the National Academy of Sciences*, vol. 116, no. 40, pp. 19 841–19 847, 2019.
- [24] N. Charles, M. Gazzola, and L. Mahadevan, "Topology, geometry, and mechanics of strongly stretched and twisted filaments: solenoids, plectonemes, and artificial muscle fibers," *Physical Review Letters*, vol. 123, p. 208003, 2019.
- [25] N. Weiner, Y. Bhosale, *et al.*, "Mechanics of randomly packed filaments - the "bird nest" as meta-material," *Journal of Applied Physics*, vol. 127, no. 5, p. 050902, 2020.
- [26] G. Sumbre, G. Fiorito, *et al.*, "Octopuses use a human-like strategy to control precise point-to-point arm movements," *Current Biology*, vol. 16, no. 8, pp. 767–772, 2006.
- [27] R. Villanueva, C. Nozais, and S. v. Boletzky, "Swimming behaviour and food searching in planktonic octopus vulgaris cuvier from hatching to settlement," *Journal of Experimental Marine Biology and Ecology*, vol. 208, no. 1-2, pp. 169–184, 1997.
- [28] R. Villanueva, V. Perricone, and G. Fiorito, "Cephalopods as predators: a short journey among behavioral flexibilities, adaptations, and feeding habits," *Frontiers in Physiology*, vol. 8, p. 598, 2017.
- [29] J. N. Richter, B. Hochner, and M. J. Kuba, "Octopus arm movements under constrained conditions: adaptation, modification and plasticity of motor primitives," *Journal of Experimental Biology*, vol. 218, no. 7, pp. 1069–1076, 2015.
- [30] —, "Pull or push? octopuses solve a puzzle problem," *PloS One*, vol. 11, no. 3, 2016.
- [31] Y. Tassa, Y. Doron, *et al.*, "Deepmind control suite," *arXiv preprint arXiv:1801.00690*, 2018.